Supramolecular Self-Assembly of Nanoconfined Ionic Liquids for Fast Anisotropic Ion Transport

Tomy Cherian, Danilo Rosa Nunes, Thomas Dane, Johan Jacquemin, Ulla Vainio, Teemu Myllymäki, Jaakko V.I. Timonen, Nikolay Houbenov, Manuel Maréchal, Patrice Rannou, et al.

Article type: Full paper

Supramolecular Self-Assembly of Nanoconfined Ionic Liquids for Fast Anisotropic Ion Transport

Tomy Cherian, Danilo Rosa Nunes, Thomas G. Dane, Johan Jacquemin, Ulla Vainio, Teemu Myllymäki, Jaakko V. I. Timonen, Nikolay Houbenov, Manuel Maréchal, Patrice Rannou, and Olli Ikkala**

T. Cherian, D. R. Nunes, Dr. U. Vainio, Dr. T. Myllymäki, Prof. J. V. I. Timonen, Dr. N. Houbenov, Prof. O. Ikkala
Department of Applied Physics
Aalto University
FI-00076 Espoo, Finland
Email: olli.ikkala@aalto.fi

Dr. M. Maréchal, Prof. O. Ikkala, Dr. P. Rannou
Univ. Grenoble Alpes, CNRS, CEA, IRIG-SyMMES
38000 Grenoble, France
Email: patrice.rannou@cea.fr

Dr. J. Jacquemin
Laboratoire PCM2E, Faculté des Sciences
Université de Tours
Parc Grandmont, 37200 Tours, France.

Materials Science and Nano-engineering,
Mohammed VI Polytechnic University,
Lot 660-Hay Moulay Rachid, Ben Guerir, Morocco.

Dr. T. G. Dane
ESRF, the European Synchrotron Radiation Facility
38000 Grenoble, France

D. R. Nunes
Laboratoire de Physique des Solides
CNRS, Université Paris-Sud, Université Paris-Saclay
91405 Orsay, France

Keywords: Ionic liquid, surfactant-self-assembly, supramolecular ionic liquid crystal, 2D ionic transport, nanoconfinement

Abstract

Materials involving nanoconfinement of ionic liquids (ILs) have been pursued for functionalities and ionic devices. However, their complex synthesis, challenges to achieve long-range order, and laborious tunability limit their practical implementation. Herein, these challenges are addressed by complexing surfactants to ILs, yielding a facile, modular, and scalable approach. Based on structural screening, ionic complexation of di-*n*-nonylamine to the terminal sulfonic acid of 1-(4-sulfobutyl)-3-methylimidazolium hydrogen sulfate IL was selected as a proof of concept. Spontaneous homeotropic smectic order over micrometers is observed, with alternating ionic and alkyl layers. The 1-nm-thick ionic layers involve 2D crystalline internal order up to 150 °C, strongly promoting anisotropic ion transport ($\sigma_{\parallel}/\sigma_{\perp}$ > 6500), and curiously, still allowing fluidity. High ionic conductivity of 35 $mS \cdot cm^{-1}$ and mesoscopic diffusion coefficient of *ca.* 10^{-5} $cm^2 \cdot s^{-1}$ at 150 °C along the ionic layers are observed. Fast anisotropic ion transport by simply complexing two components open doors to functional materials and applications.

1. Introduction

Ionic liquids (ILs) allow several functionalities and their liquid-crystalline assemblies provide anisotropic ionic conductivity.[1-7] More generally, nanoconfinement of ions can promote unusual charge transport and functionalities for IL-based devices for energy generation and storage.[8-20] On the other hand, supramolecular complexation of surfactants to polymers, block copolymers, or oligomers is a facile way to tune the self-assemblies at the nanometer length scale for functionalities.[21-27] This allows for great tunability and modularity as the molecular components can be individually engineered while the self-assemblies can be simply achieved by mixing the key components involving supramolecular interactions (*e.g.* hydrogen bonds, ionic, coordination, and halogen bonds). Such findings encouraged us to explore surfactant-induced supramolecular self-assembly of low-molecular weight IL-molecules aiming at tunable anisotropic ion transport in soft nanoconfined ionic channels. The general approach is depicted in Figure 1a using specifically ionic interactions to supramolecularly bind a surfactant (or a functional group) to the ionic liquid moiety. Driven by the high polarity differences between the polar domains of the IL and nonpolar *n*-alkyl tails of the surfactants, a well-defined segregation to self-assembled nanodomains was expected. Supramolecular modularity is inherent as the components can be engineered separately, allowing for even further complexation of functional groups to nanoconfined self-assembled ILs.

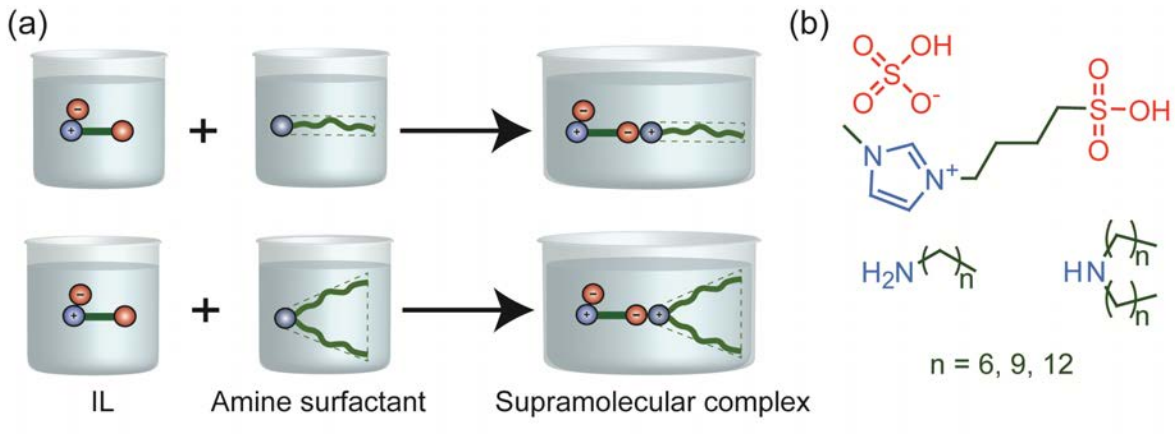

Figure 1. Modular approach for surfactant-induced self-assembly of ionic liquids. a) Scheme of electrostatic binding of a surfactant to an oppositely charged IL end group. b) 1-(4-sulfobutyl)-3-methylimidazolium hydrogen sulfate IL and the library of *n*-alkylamine and di-*n*-alkylamine surfactants used for the present supramolecular complexes.

Herein, supramolecular complexes are addressed between amine-based surfactants consisting of one- or two-tail *n*-alkylamines with chain lengths of 6, 9, and 12 methylene units and 1-(4-sulfobutyl)-3-methylimidazolium hydrogen sulfate IL (Figure 1b). The sulfonic acid end-group of the latter one is expected to ionically interact with the *n*-alkylamine and di-*n*-alkylamine surfactants upon forming an ammonium cation and a 1-(4-butylsulfonate)-3-methylimidazolium zwitterion. Zwitterions have been shown, in general, to be promising constituents to construct various functional materials.[28] The present approach leads to four charged sites for each supramolecular unit, *i.e.* particularly high polarity within the ionic domains, which we expected to promote the ionic dissociation and transport properties. It also leads to particularly strong repulsion between the alkyl and ionic layers, which we expected to promote the nanosegregation to form well-defined nanoconfined ionic layers. Furthermore, the hydrogen sulfate anion was selected to allow high overall conductivity, as suggested by the superionic protonic conductivity in the $CsHSO_4$ crystals.[29,30] Herein the phase behavior and transport properties of the complexes are investigated, where the main emphasis is to explore whether well-defined nanoconfined ionic layers can be formed *in situ* upon complexation, whether extended long-range order over micrometers can be spontaneously formed, relevant for devices, and whether high and anisotropic ionic transport can be achieved using this simple concept.

2. Results and Discussion

2.1. Supramolecular complexation of di-*n*-nonylamine with 1-(4-sulfobutyl)-3-methylimidazolium hydrogen sulfate (DiC$_9$-IL)

First, an initial screening of the complexes using different *n*-alkylamine and di-*n*-alkylamine surfactants (shown in Figure 1b) with 1-(4-sulfobutyl)-3-methylimidazolium hydrogen sulfate (IL) was performed to achieve an overall understanding on the ordering capability, thermal behavior, and transport properties. The complexes were prepared by mixing the IL/water solution with the surfactant liquid (when the surfactant was in a liquid form) or the surfactant/2-propanol solution (when the surfactant was solid), followed by a precipitation and drying (see Experimental Section for the sample preparation details and characterizations). Supporting Information shows the Fourier transform infrared spectroscopy (FTIR) and nuclear magnetic resonance (NMR) data, indicating formation of the ionic complexes between the alkylamine surfactant and IL. Supporting Information also shows a collection of physical characterization data, *i.e.*, differential scanning calorimetry (DSC), polarized optical microscopy (POM), synchrotron and in-house small and wide-angle X-ray scatterings (SAXS/WAXS), and electrochemical impedance spectroscopy (EIS) data.

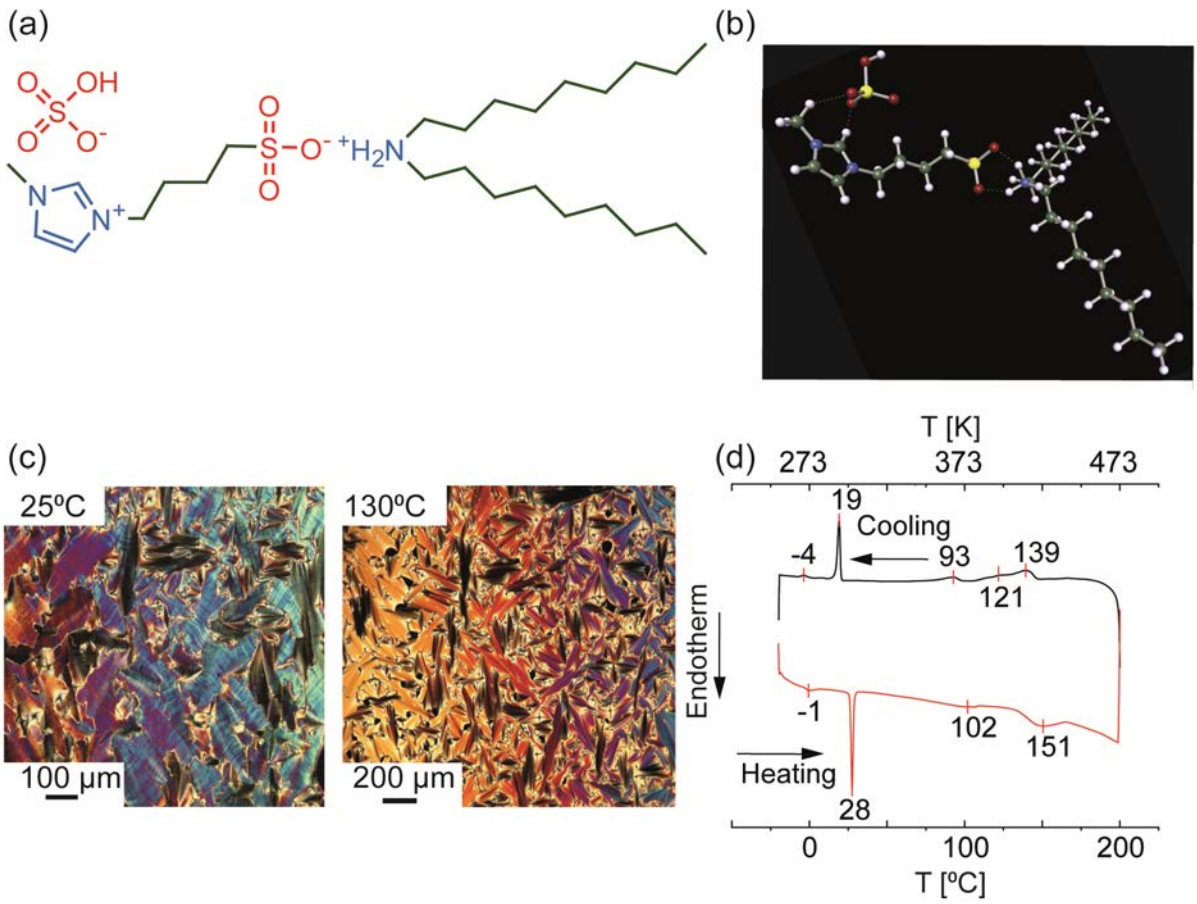

Figure 2. Supramolecular ionic complex di-*n*-nonylamine 1-(4-sulfobutyl)-3-methylimidazolium hydrogen sulfate (DiC_9-IL). a) The expected "double ionic complex" in DiC_9-IL. b) The isolated supramolecular complex DiC_9-IL based on DFT calculations (HF/6-311++G** based on DFT/B3LYP/def-TZVP-RI in gas phase). c) Polarized optical micrographs of DiC_9-IL at 25 °C (permanently arced focal-conic fan texture) and 130 °C (focal-conic fan texture) qualitatively suggesting smectic phases. d) DSC showing a sequence of enantiotropic phases as a function of temperature. Note that DiC_9-IL was stable up to *ca.* 150 °C, allowing lengthy experimentations below such a temperature. However, the rapid temperature sweep rate of 10 °C·min^{-1} allowed quick probing of even higher temperatures using DSC where degradation was otherwise observed.

Among the alkylamine surfactants, di-*n*-nonylamine turned particularly feasible, aiming at sufficient fluidity at elevated temperatures to fill the liquid crystal (LC) cells in combination with high order and ionic transport. Therefore, di-*n*-nonylamine 1-(4-sulfobutyl)-3-

methylimidazolium hydrogen sulfate, denoted subsequently as DiC_9-IL (see Figures 2a-b) was selected for detailed experimental and simulation studies. Importantly, DiC_9-IL was an easily flowing fluid at 150 °C (see Figure S27, Supporting Information), however, it became highly viscous and solid upon approaching the room temperature. The crystallization and melting temperatures are *ca.* 19 and 28 °C based on DSC thermograms, respectively (Figure 2d). POM showed birefringent colorful focal-conic fan textures, suggesting smectic layered phases, see Figure 2c for the POM patterns at 25 and 130 °C. Still a subtlety existed: characteristically such birefringent POM patterns were not observed, not due to the lack of the order, but due to a pronounced tendency to spontaneously form nonbirefringent homeotropically aligned mesophases involving ionic layers parallel to the substrate. Indeed, POM images like in Figure 2c required specific manipulation of the matter to create the defects and the birefringence. In fact, we considered the tendency to form homeotropic alignment as particularly beneficial towards the long-range order. Another subtlety was that the structures were, in fact, more complex than those of the classic smectics, as the present materials involved alternating alkyl layers and 2D ionic crystalline layers, as the structural analysis later in this report shows. A final subtlety is that an isotropic state was not observed using POM upon sufficient heating, which is at first slightly surprising. However, this is a manifestation that the isotropic state is achieved at the temperatures where a concurrent chemical degradation starts to be relevant. In fact, this is not surprising taken the high repulsion between the ionic and alkyl layers, leading to pronounced stabilization of the layered smectic phases, thus increasing the transition temperature to the isotropic state. Therefore, the material turned stable enough up to 150 °C to allow the lengthy POM measurements, but started to show some degradation upon prolonged stay already beyond *ca.* 155 °C (see Figure S25, Supporting Information). However, rapid temperature sweeps up to higher temperatures were still feasible, and thus allowed temperatures up to 200 °C quickly to be probed. Thus, DSC using rapid sweep rates of 10 $°C \cdot min^{-1}$ indicated the isotropic phase and several enantiotropic phase transitions in cooling and heating (see

Figure 2d). Note that the phase transition temperatures suggested by the DSC with its high sweep rate cannot directly be compared with the phase transition temperatures observed using POM or X-ray studies, which require small temperature sweep rates to reach the equilibrium. That DSC showed several phase transitions was, in fact, not surprising, as seen for other imidazolium ILs with an HSO_4^--counter-anion.[31]

2.2. Structures of DiC_9-IL

Figure 3a shows the measured SAXS/WAXS pattern at 25 °C as a function of the scattering-vector modulus $q = (4\pi/\lambda)\cdot\sin\theta$, where 2θ is the scattering angle (see Experimental Section). Two major reflections at low angles are observed, $q = 2.84$ nm^{-1} and 3.23 nm^{-1} as well as a large number of higher order reflections. The structure was assigned using direct-space methods based on the X-ray reflections and retrostructurally it was geometry-optimized using a DFT approach to clarify whether such a structure leads to minimization of energy (see Experimental Section and Supporting Information).[32-37] The observed SAXS/WAXS 1D pattern matches with the suggested structure with the two main reflections at $q = 2.84$ nm^{-1} and 3.23 nm^{-1} being assigned to the *c* and *a* directions of the monoclinic unit cell, respectively (Figure 3a inset). Figure 3b shows the calculated energy minimized structure and Figure 3c schematically visualizes the structure in a simplified form. The structure consists of alternating alkyl and ionic layers of less than 1 nm in thickness. The zwitterion moiety 1-(4-butylsulfonate)-3-methylimidazolium involves a large electric dipole moment and hence they pack antiparallel within the ionic layers. The di-*n*-nonylammonium cation binds close to the sulfonate of 1-(4-butylsulfonate)-3-methylimidazolium and to the hydrogen sulfate anion. The HSO_4^--counter-ion has interesting hydrogen bonding donor (-S-OH) and acceptor (-S=O) functionalities. This has previously led to hydrogen bonded HSO_4^--chains in $CsHSO_4$ at low temperatures.[30] Furthermore, in other imidazolium ILs, this counter-ion has a strong role to control the assembly due to formation of hydrogen bonds between the counter-ions.[31,38] Not surprisingly, also in the

present DiC_9-IL, the calculated structure suggests formation of hydrogen bonded chains of HSO_4^- in the *b*-direction with S-S distances of 0.4 nm and corresponding H-bond distance of 0.14 nm (Figure S9, Supporting Information).

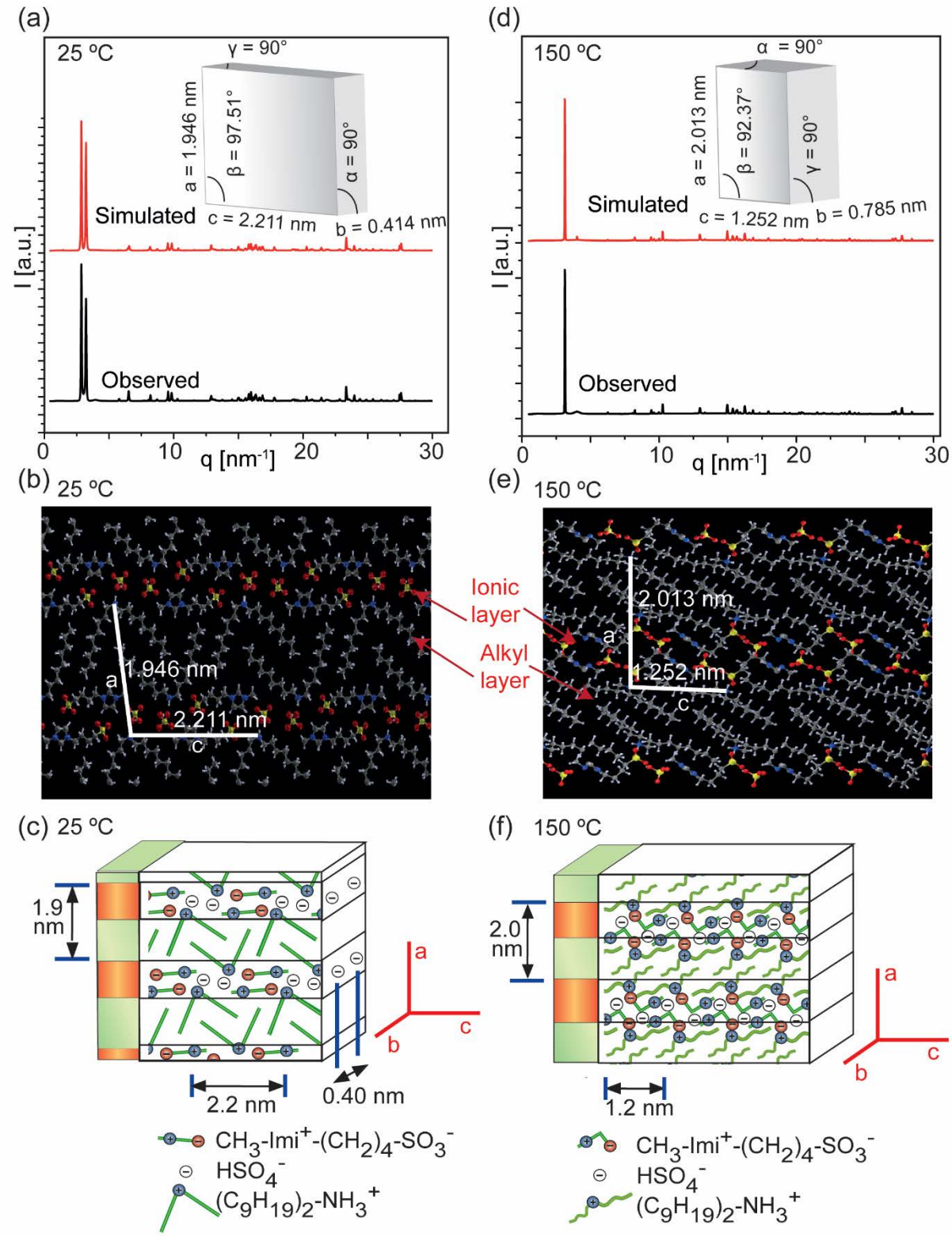

Figure 3. Structures of DiC_9-IL at two temperatures. a) Synchrotron SAXS/WAXS 1D patterns measured at 25 °C, compared with the calculated patterns based on the simulated structure shown in b) based on geometry-optimization by DFT. The inset shows the monoclinic unit cell at 25 °C. c) Schematic structure at 25 °C. d) Synchrotron SAXS/WAXS 1D pattern measured at 150 °C, compared with the calculated pattern based on the structure shown in e), geometry-optimized by DFT. The inset shows the monoclinic unit cell at 150 °C. f) Schematic structure at 150 °C.

Figure 3d discloses the measured SAXS/WAXS 1D pattern at 150 °C. It shows one intense reflection at q = 3.12 nm^{-1} and a large number of reflections at higher scattering angles. The molecular packing was again calculated suggesting a monoclinic unit cell (Figure 3e and Figure S10, Supporting Information), matching the observed scattering peaks (Figure 3d). The structure again indicates a smectic supramolecular ionic liquid crystal with alternating ionic and alkyl layers. Figure 3f schematically illustrates the packing. The zwitterionic moiety 1-(4-butylsulfonate)-3-methylimidazolium adopts now a kink, allowed by the *cis-trans* conformations of the flexible butyl spacer. Related kinked conformation has previously been suggested for other compounds.[39] A landmark feature is that the nanoconfined ionic layers form internal 2D crystalline order even at 150 °C (see Figure 3d), and the material is still able to flow (see Figure S27, Supporting Information). Related seemingly contradicting combination of 2D-crystalline nanoscale order in smectics and simultaneous flow has been observed previously in rare cases and is here supported by the molten di-*n*-alkyl tails (see Figure S28, Supporting Information).[40]

2.3. Ion transport of DiC_9-IL, based on electrochemical impedance spectroscopy (EIS)

The ionic transport is next addressed. Note that these supramolecular complexes have the attractive feature that they spontaneously form homeotropically aligned mesophases on glass or ITO-coated glass plates with parallel ionic layers (see Figure 3) *vs.* the substrate, thus

obviously facilitating extended long-range smectic order. Parallel *vs.* perpendicular ionic transport was explored with two types of LC cells (Figures 4a *vs.* 4b and Supporting Information). The LC cells were spontaneously filled at 120-150 °C due to capillary action, as allowed by the high temperature fluidity, addressed above (Figure S27, Supporting Information). The homeotropic alignment of the mesophase was assessed using *in-situ* POM. The EIS diagrams were fitted and analyzed with models described in the Supporting Information.

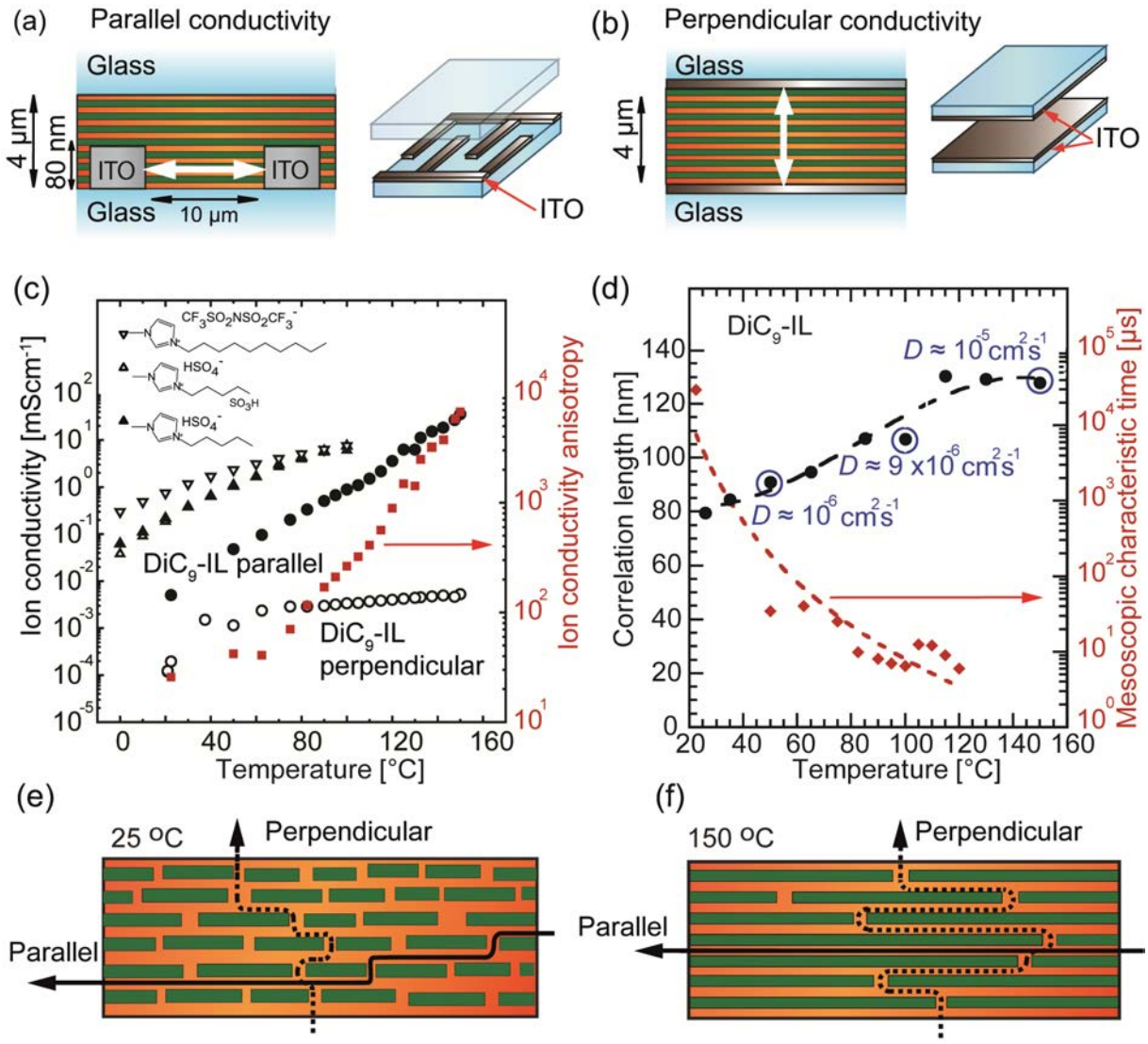

Figure 4. Ion transport of DiC_9-IL, based on electrochemical impedance spectroscopy (EIS). The sample cell geometries to study the ionic transport in a) parallel and b) perpendicular directions *vs.* the glass substrate with ITO electrodes. c) The parallel and perpendicular ion

transport and transport anisotropy of DiC_9-IL. The low temperature kink in the perpendicular geometry is probably reflecting the effect of the crystallization of the di-*n*-alkyl chains, thus leading to reduced electrical contact. As a reference, the ionic conductivities of non-self-assembled ILs 1-(4-sulfobutyl)-3-methylimidazolium hydrogen sulfate, 1-butyl-3-methylimidazolium hydrogen sulfate and 1-decyl-3-methylimidazolium bis[(trifluoromethyl)sulfonyl]imide are shown. d) Correlation lengths parallel to the ionic layers and the mesoscopic (*ca.* μm scale) characteristic times of ion transport as a function of the temperature for DiC_9-IL. Diffusion coefficients calculated from EIS data are shown at 50, 100 and 150 °C. e) Schematics of the 2D ion transport at 25 °C. f) Schematics of the 2D ion transport at 150 °C, respectively. The correlation length parallel to ionic layers increases up to 150 °C, improving the ion transport in the parallel direction. The ion transport in perpendicular direction is likely due to structural defects inducing leakage of ions through cascading nanoslits in the direction perpendicular to ionic layers.

Before addressing the most remarkable observed transport feature of DiC_9-IL, *i.e.,* the high charge carrier diffusion coefficient *D*, Figure 4c depicts the ionic conductivity parallel and perpendicular to the ionic layers as a function of temperature. The parallel conductivity is high, reaching 1 $mS \cdot cm^{-1}$ at 100 °C and up to 35.5 $mS \cdot cm^{-1}$ at 150 °C. Figure 4c also depicts the bulk conductivity of reference imidazolium ionic liquids, classical isotropic electrolytes not involving ionic layer nanoconfinement: pure 1-(4-sulfobutyl)-3-methylimidazolium hydrogen sulfate, 1-butyl-3-methylimidazolium hydrogen sulfate and 1-decyl-3-methylimidazolium bis[(trifluoromethyl)sulfonyl]imide. Interestingly, their ultimate conductivity at elevated temperatures (*i.e.* $T > 120$ °C) remains inferior to DiC_9-IL, directly confirming the advantageous effects of 2D nanoconfinement and long-range organization to promote ionic transport. Additionally, the parallel conductivity of DiC_9-IL at 150 °C is higher than the conductivity in the superionic state (140 - 200 °C) of $CsHSO_4$ crystals (1-10 $mS \cdot cm^{-1}$).[29] It

also compares favorably with the state-of-the-art 2D ionic liquid crystals and poly(ionic liquids) at 100 °C.[6,41]

Uncommon observations are involved in the transport properties. First, the parallel conductivity substantially increases with the temperature but the perpendicular conductivity is low and increases only slightly as a function of the temperature (Figure 4c). Therefore, the anisotropy $\sigma_{\parallel}/\sigma_{\perp}$ constantly increases with the temperature, reaching up to 3.5 orders of magnitude (*ca.* 6500) at 150 °C (Figure 4c). Such an anisotropy value is high, but it is even more striking that the anisotropy increases towards the highest temperatures. This behavior seems to be against the common behavior where the anisotropy vanishes at the highest temperatures where the isotropic phase is achieved. However, in the present case the lengthy transport measurements cannot be extended to the isotropic phase as thermal degradation starts to take place above > 155 °C. Another subtlety is involved in the temperature behaviors of the conductivities. Figure 3a showed a strong X-ray reflection at q = 2.84 nm^{-1} which shifts to q = 3.12 nm^{-1} upon heating from 25 to 150 °C (Figure S13, Supporting Information). It was assigned to the periodicity in the *c*-direction (parallel to substrate). The related peak width (Figure S13, Supporting Information) allows the estimation of the correlation length in the parallel *c*-direction (Figure 4d, see Supporting Information for details). It increases upon heating, which at first sight seems paradoxical. However, in order to achieve perfect lamellar order, the lateral cross-sectional areas of the corresponding ionic and alkyl moieties (in the lamellar direction) should exactly match to avoid packing frustrations. Packing frustrations can, in general, be relieved by forming granular domains. In the present case, the increased fluidity and ability for molecular rearrangements upon heating allows to relieve such packing frustrations at high temperatures for promoted long-range structural order in DiC_9-IL. Simultaneously, the mesoscopic characteristic times (Figure 4d), extracted from EIS, decrease with temperature (see Supporting Information for details). All these observations indicate increasing long-range order upon heating, and consequently, promoted-ion transport parallel to the ionic layers with

temperature (Figures 4e-f). Even more interestingly, the ionic diffusion coefficients obtained with correlation lengths and mesoscopic characteristic times of the ionic transport (Figure 4d) are *ca*. $9 \cdot 10^{-6}$ $cm^2 \cdot s^{-1}$ at 100 °C and *ca.* 10^{-5} $cm^2 \cdot s^{-1}$ at 150 °C, which exceeds, *e.g*., the state-of-the-art hydroxonium diffusion coefficient in high performance polymer electrolyte membranes[15] (see Figures S19-S22 in Supporting Information for characteristic times of other complexes). It is striking to reach beyond the state-of-the art values using such a simple procedure.

On the contrary, perpendicular conductivity reaches a plateau value around 120 °C; a behavior that is common for all the supramolecular complexes in this family (Figure 4c and Figure S24, Supporting Information). The perpendicular conductivity is most likely governed by a cascading mechanism through nanoslit defects (leakage channels) across the ionic layers (Figures 4e-f). The higher the number of these leakage channels, the easier it is for an ion to escape and hop from an ionic 2D-pathway up or down to another equivalent one. The plateau at high temperatures could then be explained by the long-range ordering of the 2D ionic pathways disadvantaging the perpendicular cascading mechanism. Schematic illustration of this 2D ion transport with leakage channels is shown in Figures 4e-f.

3. Conclusion

In summary, we show that supramolecular complexation of a surfactant to an ionic liquid allows a facile and modular route to control the self-assemblies to form ionic liquid crystals by simply mixing them, leading to nanoconfined smectic ionic layers with internal 2D crystalline order for fast anisotropic ion transport. Surprisingly, the alternating layered 2D ionic crystals of thickness of *ca.* 1 nm separated by *ca.* < 1 nm alkyl layers allow fluid mesophases at elevated temperatures. As the ionic layers are highly polar due to the presence of four sites of charges for each supramolecular unit within the nanoconfinement, sufficient repulsion to allow the smectic self-assembly is expected to generalize the present concept by replacing the surfactant alkyl tails by more functional units. Furthermore, the IL counter-ion can be changed (or can be

a combination of different anions) to improve for example the hydrophobicity or the proton hoping of the targeted complexes. The 2D long-range ordered nanoconfinement with efficient local charged space allows to reach higher ultimate conductivities and anisotropies upon heating than the corresponding bulk ILs, demonstrating clearly the main advantage of soft nanoconfinement-based materials. This 2D fast ion transporting material offers potential applications as electrolyte in future energy storage and conversion devices such as supercapacitors[42] and batteries.

4. Experimental Section

Detailed experimental methods are disclosed in the Supporting Information.

Preparation of self-assembled surfactant-induced ionic liquid complexes: The *n*-alkylamines and di-*n*-alkylamines, which are liquid at room temperature, *i.e.* the *n*-hexylamine (Fluka, purity 98%, CAS number: [111-26-2]), *n*-nonylamine (Sigma-Aldrich, purity 98 %, CAS number: [112-20-9]), di-*n*-hexylamine (Sigma-Aldrich, purity 97 %, CAS number: [143-16-8]), were added directly to equimolar quantity of 1-(4-sulfobutyl)-3-methylimidazolium hydrogen sulfate (IL, Solvionics (Ref ImSF1213c), www.solvionic.com, 98 % purity, CAS number: [827320-59-2]) dissolved in H_2O (4 mg·mL^{-1}). The *n*-alkylamines and di-*n*-alkylamines, which are solid at room temperature (*i.e. n*-dodecylamine (Fluka, purity 99.5 %, CAS number: [124-22-1]), di-*n*-nonylamine (Gentaur, purity 97 %, CAS number: [2044-21-5], di-*n*-dodecylamine (Sigma-Aldrich, purity 97 %, CAS number: [3007-31-6]) were first dissolved in 2-propanol (2 mg.mL^{-1}) before mixing with aqueous solution of IL. In both cases, the complexes are obtained by mixing an equimolar amount of *n*-alkylamine (or di-*n*-alkylamine) and IL. This mixing induced then a slow precipitation of the complexes, result of an acid-base reaction between the sulfobutyl moiety of the former IL and the selected amine. In order to ensure complete complexation, the solution was mixed in a rotor for ~24 hrs. The complexes were then fully

extracted from the solution by rotary evaporation. The complexation was confirmed with FTIR and NMR as shown in the Supporting Information.

Small/Wide angle X-ray scatterings (SAXS/WAXS) measurements and analysis: Temperature-dependent SAXS/WAXS measurements were carried out on bulk samples using synchrotron facility (ID13 and BM02-D2AM beamlines, ERSF, Grenoble, France) and an in-house line (IRIG/DEPHY/MEM/SGX, Grenoble, France). The scattered X-ray patterns were recorded on the microfocus ID13 beamline (energy E = 13 keV, wavelength λ = 9.537 nm), the BM02-D2AM SAXS/WAXS beamline (E = 24 keV, λ = 0.057 nm) and an in-house setup (E = 8 keV, λ = 0.15118 nm). The reflections were fitted with Gaussian functions to analyze the peaks.

Structure simulation: X-ray patterns were indexed using N-TREOR09 in EXPO2014 after manual selection of peaks.[43,44] Simulated annealing was performed using EXPO2014 with all fragments set up as rigid bodies, except for di-*n*-nonylamine where secondary amine and adjacent carbons were allowed to move freely between them. All models were then subject to geometry optimization using the Relax function of the DFT package Quantum espresso (method BFGS) with fixed cell parameters.[45,46] Rietveld refinement was performed in all models using EXPO2014 with all fragments set as rigid bodies.[44,47,48]

Ion transport measurement and analysis: Ion transport measurements were carried out using an HF2IS impedance spectroscope (Zurich Instruments). The samples were first filled in LC cells (Instec Inc.) at high temperatures allowing easy flow. Parallel ion transport (along the ionic layers) was measured using cells with interdigitated in-plane ITO electrodes on glass substrate. Perpendicular ion transport (across the ionic layers) was measured using cells containing parallel ITO electrodes (sandwich configuration) on glass substrates (schemes shown in Figures 4a-b). The EIS diagrams were recorded during slow cooling scans (0.5 °C·min^{-1} unless noted otherwise) between 5 Hz and 10 MHz using an ac-excitation of 100 mV with a temperature controlled at ±0.1 °C. The raw data were imported to the Zview software (Scriber Associates Inc.) for further analyses described in detail in the Supporting Information. The low frequency

region of the impedance diagrams in the electrochemistry Nyquist plot showed an inclined straight line and the high frequency region showed a depressed semi-circle. The data were fitted with appropriate phenomenological models (see Supporting Information). A parallel circuit with a resistance and a constant phase element is an adequate model of the supramolecular complexes between blocking electrodes. The first one represents the dissipative contributions of the dielectric response, while the second one describes the ability of the dielectric component to store the electric field through polarization mechanisms.

Supporting Information

Supporting Information is available from the Wiley Online Library or from the authors.

Acknowledgements

P.R. and O.I. conceived the concept. T.C., P.R., M.M., and N.H. made the samples. T.C, M.M., T.G.D., N.H., P.R., T.M., J.T. and U.V. made the characterization, D.R.N. and J.J. made the DFT modelling. O.I. and P.R. wrote the first version of the article; all authors contributed to the interpretations and commented on the manuscript. The authors are grateful for financial support by ERC Advanced Grant, Academy of Finland, and the Centre National de la Recherche Scientifique (CNRS) at the laboratoire des Systèmes Moléculaires et nanoMatériaux pour l'Énergie et la Santé in Grenoble (France) [UMR5819-SyMMES (CNRS/CEA/UGA)]. The authors thank Nanomaterials of Aalto University for the support. We acknowledge the facilities and technical support by Aalto University at OtaNano - Nanomicroscopy Centre (Aalto-NMC), and the technical supports, local contacts and the fruitful helps and discussions on the Large Scale Facilities including M. Burghammer and M. Sztucki (ESRF/ID13 microfocus beamline), I. Morfin, N. Boudet, and N. Blanc (ESRF/BM02-D2AM beamline), A. De Geyer and S. Lequien (home-made SAXS/WAXS setup at IRIG/DEPHY/MEM/SGX), and W. Briscoe (University of Bristol) for complementary XRD measurements on ESRF/BM28.

Conflict of Interest

The authors declare no conflict of interest.

Keywords

Ionic liquid, surfactant-self-assembly, supramolecular ionic liquid crystal, 2D ionic transport, nanoconfinement

Received: ((will be filled in by the editorial staff))
Revised: ((will be filled in by the editorial staff))
Published online: ((will be filled in by the editorial staff))

References

[1] T. Welton, *Chem. Rev.* **1999**, *99*, 2071.

[2] J. P. Hallett, T. Welton, *Chem. Rev.* **2011**, *111*, 3508.

[3] M. Armand, F. Endres, D. R. MacFarlane, H. Ohno, B. Scrosati, *Nat. Mater.* **2009**, *8*, 621.

[4] K. Goossens, K. Lava, C. W. Bielawski, K. Binnemans, *Chem. Rev.* **2016**, *116*, 4643.

[5] M. Yoshio, T. Mukai, K. Kanie, M. Yoshizawa, H. Ohno, T. Kato, *Adv. Mater.* **2002**, *14*, 351.

[6] J. Sakuda, M. Yoshio, T. Ichikawa, H. Ohno, T. Kato, *New J. Chem.* **2015**, *39*, 4471.

[7] T. Kato, M. Yoshio, T. Ichikawa, B. Soberats, H. Ohno, M. Funahashi, *Nat. Rev. Mater*. **2017**, *2*, 17001.

[8] S. Zhang, J. Zhang, Y. Zhang, Y. Deng, *Chem. Rev.* **2017**, *117*, 6755.

[9] J. Maier, *Nat. Mater.* **2005**, *4*, 805.

[10] J.-J. Shao, K. Raidongia, A. R. Koltonow, J. Huang, *Nat. Commun*. **2014**, *6*, 7602.

[11] A. R. Koltonow, J. Huang, *Science* **2016**, *351*, 1395.

[12] C. Cheng, G. Jiang, C. J. Garvey, Y. Wang, G. P. Simon, J. Z. Liu, D. Li, *Sci. Adv.* **2016**, *2*, e1501272.

[13] P. Sun, R. Ma, X. Bai, K. Wang, H. Zhu, T. Sasaki, *Sci. Adv.* **2017**, *3*, e1602629.

[14] R. Futamura, T. Iiyama, Y. Takasaki, Y. Gogotsi, M. J. Biggs, M. Salanne, J. Ségalini, P. Simon, K. Kaneko, *Nat. Mater.* **2017**, *16*, 1225.

[15] E. B. Trigg, T. W. Gaines, M. Maréchal, D. E. Moed, P. Rannou, K. B. Wagener, M. J. Stevens, K. I. Winey, *Nat. Mater.* **2018**, *17*, 725.

[16] N. Kavokine, S. Marbach, A. Siria, L. Bocquet, *Nat. Nanotechnol.* **2019,** *14*, 573.

[17] N. Gao, Y. He, X. Tao, X.-Q. Xu, X. Wu, Y. Wang, *Nat. Commun.* **2019**, *10*, 547.

[18] J. Yang, X. Hu, X. Kong, P. Jia, D. Ji, D. Quan, L. Wang, Q. Wen, D. Lu, J. Wu, L. Jiang, W. Guo, *Nat. Commun.* **2019**, *10*, 1171.

[19] T. Li, X. Zhang, S. D. Lacey, R. Mi, X. Zhao, F. Jiang, J. Song, Z. Liu, G. Chen, J. Dai, Y. Yao, S. Das, R. Yang, R. M. Briber, L. Hu, *Nat. Mater.* **2019**, *18*, 608.

[20] D. R. MacFarlane, M. Forsyth, P. C. Howlett, M. Kar, S. Passerini, J. M. Pringle, H. Ohno, M. Watanabe, F. Yan, W. Zheng, S. Zhang, J. Zhang, *Nat. Rev. Mater.* **2016**, *1*, 1.

[21] B. Dufour, P. Rannou, D. Djurado, H. Janeczek, M. Zagorska, A. de Geyer, J.-P. Travers, A. Pron, *Chem. Mater.* **2003**, *15*, 1587.

[22] C. F. J. Faul, M. Antonietti, *Adv. Mater.* **2003**, *15*, 673

[23] C. F. J. Faul, *Acc. Chem. Res.* **2014**, *47*, 3428.

[24] O. Ikkala, G. ten Brinke, *Science* **2002**, *295*, 2407.

[25] N. Houbenov, R. Milani, M. Poutanen, J. Haataja, V. Dichiarante, J. Sainio, J. Ruokolainen, G. Resnati, P. Metrangolo, O. Ikkala, *Nat. Commun.* **2014**, *5*, 4043.

[26] O. Ikkala, N. Houbenov, P. Rannou, In *Handbook of Liquid Crystals*; Wiley-VCH Verlag GmbH & Co. KGaA: Weinheim, Germany, **2014,** pp. 541-598.

[27] Y. Zhou, M. Antonietti, *Adv. Mater*. **2003**, *15*, 1452.

[28] T. Ichikawa, *Polym. J.* **2017**, *49*, 413.

[29] A. I. Baranov, L. A. Shuvalov, N. M. Shchagina, *JETP Lett.* **1982**, *36*, 459.

[30] M. Pham-Thit, Ph. Colomban, A. Novak, R. Blinc, *J. Raman Spectrosc.* **1987**, *18*, 185.

[31] L. F. O. Faria, T. A. Lima, F. F. Ferreira, M. C. C. Ribeiro, *J. Phys. Chem. B* **2018**, *122*, 1972.

[32] R. Ahlrichs, M. Bär, M. Häser, H. Horn, C. Kölmel, *Chem. Phys. Lett.* **1989**, *162*, 165.

[33] F. Weigend, M. Häser, *Theor. Chem. Acc.* **1997**, *97*, 331.

[34] F. Weigend, M. Häser, H. Patzelt, R. Ahlrichs, *Chem. Phys. Lett.* **1998**, *294*, 143.

[35] A. D. Becke, *Phys. Rev. A* **1988**, *38*, 3098.

[36] C. Lee, W. Yang, R. G. Parr, *Phys. Rev. B* **1988**, *37*, 785.

[37] S. Grimme, *J. Comput. Chem.* **2006**, *27*, 1787.

[38] P. Kölle, R. Dronskowski, *Inorg. Chem.* **2004**, *43*, 2803.

[39] X.-M. Liu, Z.-X. Song, H.-J. Wang, *Struct. Chem.* **2009**, *20*, 509.

[40] M. Arkas, I. Kitsou, F. Petrakli, *Liq. Cryst.* **2018**, *45*, 70.

[41] A. Jourdain, A. Serghei, E. Drockenmuller, *ACS Macro Lett.* **2016**, *5*, 1283.

[42] X. Mao, P. Brown, C. Červinka, G. Hazell, H. Li, Y. Ren, Di. Chen, R. Atkin, J. Eastoe, I. Grillo, A. A. H. Padua, M. F. Costa Gomes, T. A. Hatton, *Nat. Mater.* **2019**. DOI: 10.1038/s41563-019-0449-6

[43] A. Altomare, G. Campi, C. Cuocci, L. Eriksson, C. Giacovazzo, A. Moliterni, R. Rizzi, P.-E. Werner, *J. Appl. Crystallogr.* **2009**, *42*, 768.

[44] A. Altomare, C. Cuocci, C. Giacovazzo, A. Moliterni, R. Rizzi, N. Corriero, A. Falcicchio, *J. Appl. Crystallogr.* **2013**, *46*, 1231.

[45] P. Giannozzi, S. Baroni, N. Bonini, M. Calandra, R. Car, C. Cavazzoni, D. Ceresoli, G. L. Chiarotti, M. Cococcioni, I. Dabo, A. Dal Corso, S. de Gironcoli, S. Fabris, G. Fratesi, R. Gebauer, U. Gerstmann, C. Gougoussis, A. Kokalj, M. Lazzeri, L. Martin-Samos, N. Marzari, F. Mauri, R. Mazzarello, S. Paolini, A. Pasquarello, L. Paulatto, C. Sbraccia, S. Scandolo, G. Sclauzero, A. P. Seitsonen, A. Smogunov, P. Umari, R. M. Wentzcovitch, *J. Phys. Condens. Matter* **2009**, *21*, 395502.

[46] P. Giannozzi, O. Andreussi, T. Brumme, O. Bunau, M. Buongiorno Nardelli, M. Calandra, R. Car, C. Cavazzoni, D. Ceresoli, M. Cococcioni, N. Colonna, I. Carnimeo, A. Dal Corso, S. de Gironcoli, P. Delugas, R. A. DiStasio, A. Ferretti, A. Floris, G. Fratesi, G. Fugallo, R. Gebauer, U. Gerstmann, F. Giustino, T. Gorni, J. Jia, M. Kawamura, H.-Y. Ko, A. Kokalj, E. Küçükbenli, M. Lazzeri, M. Marsili, N. Marzari, F. Mauri, N. L. Nguyen, H.-V. Nguyen, A. Otero-de-la-Roza, L. Paulatto, S. Poncé, D. Rocca, R. Sabatini, B. Santra, M. Schlipf, A. P. Seitsonen, A. Smogunov, I. Timrov, T. Thonhauser, P. Umari, N. Vast, X. Wu, S. Baroni, *J. Phys. Condens. Matter* **2017**, *29*, 465901.

[47] H. M. Rietveld, *J. Appl. Crystallogr.* **1969**, *2*, 65.

[48] L. B. McCusker, R. B. Von Dreele, D. E. Cox, D. Louër, P. Scardi, *J. Appl. Crystallogr.* **1999**, *32*, 36.